# Development of a Low Head Tidal Turbine
# Part 1: CFD Simulations, Design and Optimization

Stephan Hötzl[*1], Tobias Schechtl[*2], Peter Rutschmann[*3] and Wilfried Knapp[*4]

*Chair of Hydraulic and Water Resources Engineering
Technical University of Munich
Arcisstraße 21, Munich, Germany
[1]stephan.hoetzl@tum.de
[2]tobias.schechtl@tum.de
[3]peter.rutschmann@tum.de
[4]wilfried.knapp@tum.de

*Abstract*—**Recent research has shown that four-quadrant turbines are required to achieve maximum net energy production in a tidal barrage plant. These turbines can generate electricity in both flow directions and are capable of pumping. An innovative turbine concept is being reviewed in the course of the Eurostars research project Safe\*Coast. This project proposes to install a turbine in a reversible cylinder in order to allow for four-quadrant operation. To evaluate the feasibility of the concept, the authors designed a compact low head axial tidal turbine with the aid of CFD simulations.**

**This paper presents the methods used in the design and optimization process of the turbine. It also describes numerically obtained turbine characteristics, and cavitation limits. The most critical requirements of the turbine include high efficiency in turbine and pumping mode and safe cavitation properties. By computing steady state CFD simulations of the turbine stage, an extensive set of geometries was analyzed. The authors optimized the turbine performance by adjusting the meridional section, as well as runner blade and guide vane profiles and angles along with other related parameters. Transient simulations of the whole setup, including the inlet and draft tube geometries, were performed in order to study transient effects.**

**The final design after optimization is a three bladed axial turbine with adjustable guide vanes and a rim generator. The turbine's symmetrical inlet and outlet geometry and its relative compactness permit its integration in a reversible cylinder. The simulation results are very positive and indicate that all the relevant design criteria are satisfied. As a result, the project will continue into a new phase in which a model of the turbine will be built for physical testing in order to verify the results and to conduct further investigations.**

*Index Terms*—**Tidal Turbine, Computational Fluid Dynamics, Hydraulic Machines, CFD Simulations, Tidal Energy, Pump Turbine**

## I. INTRODUCTION

The generation of energy from tides has been practiced since ancient times [1]. First applications were tidal mills that were used to grind corn in order to produce flour. The oldest known tidal mill was on Mahee Island in northern Ireland and has been dated by dendrochronology to 619-621 AD [2]. It used the potential energy of seawater between high and low tide. A dam separated a reservoir from the sea and the difference in water levels caused a flow, which in turn drove water wheels. This was thus the first implementation of what

is these days termed a tidal barrage power plant these days. An alternative concept, that uses the kinetic energy of flowing water, is tidal stream turbines. Much research has been put into the development of tidal stream turbines, but tidal barrage power plants still produce the lion's share of electricity from tides.

All major tidal power plants in operation generate electricity with the use of a barrage and turbines. Kaplan bulb turbines, where the generator is located inside a bulb upstream of the runner, are the most commonly used type. In the Annapolis tidal power plant in Canada, a Straflo turbine is installed, which is an alternative design that uses a rim generator [3]. Another exception is the Kislaya Guba tidal power station in Russia, where old Kaplan-bulb units were replaced by orthogonal turbines. An overview of the turbines used in existing tidal power stations is given in Table I.
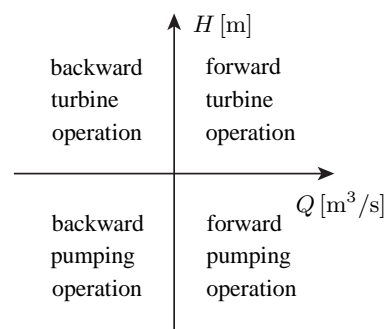


Fig. 1. Four quadrants of turbine operation

Figure 1 shows the four modes in which a hydraulic turbine can operate. The most frequently used and therefore most important mode is the forward turbine mode, for which a turbine is usually optimized. In this case, the water flows through the turbine in the optimal direction, driven by the hydraulic head. The turbine generates most power at its greatest efficiency and maximum output. If the hydraulic head is reversed, which happens regularly in two-way-operation, the flow direction is also reversed. The efficiency in the reverse operation is lower due to the two main disadvantages of bulb turbines.

TABLE I
TURBINES USED IN EXISTING TIDAL POWER PLANTS

| | Diameter [m] | Head [m] | Discharge [m³/s] | n · Power [MW] | Turbine type |
|---|---|---|---|---|---|
| La Rance [4] | 5.35 | rated: 5.65 | rated: 275 | 24 · 10 | Bulb turbine |
| Annapolis [4] | 7.60 | rated: 5.50 range: 1.4-7.1 | max: 407.5 rated: 378 | 1 · 19.6 | Straflo turbine |
| Kislaya Guba old [5] | 3.30 | rated: 1.28 range: 0.5-2.5 | rated: 50 | 1 · 0.4 | Bulb turbine |
| Kislaya Guba new [6] | 2.50 5.00 | n/a n/a | n/a n/a | 1 · 0.2 1 · 1.5 | Orthogonal turbine |
| Sihwa-Ho [7] | 7.50 | rated: 5.82 range: 2.0-6.0 | max: n/a rated: 482 | 10 · 25.4 | Bulb turbine |
| Jiangxia [8] | 2.50 | rated: 3.00 range: 1.2-5.5 | max: 34 rated: 29.7 | 1 · 0.545 1 · 0.655 4 · 0.760 | Bulb turbine |

Firstly, the generator bulb is situated in the downstream flow of the runner. Flow separation occurs behind the bulb and thus the draft tube efficiency is significantly impaired. Secondly, the guide vanes are now placed downstream of the runner, instead of upstream. Therefore, no inlet swirl can be generated and the guide vanes need to remove the runner outlet swirl, which can be problematic due to the low pressure in this region. For these two reasons, it is inherently impossible to achieve the same efficiency in reverse mode, even with careful optimization. If pumping is also required in the operation scheme, this adds a further complication. Adapting a turbine to deliver satisfactory efficiency as a pump in the reversed flow direction already calls for some compromise, but achieving high efficiency in the forward pumping mode would require differently shaped runner blades and guide vanes. Due to these conflicting hydrodynamic requirements, a turbine cannot be optimized for all four modes.

The turbines in the La Rance tidal power plant were commissioned in 1967. Their greatest efficiency is 87 % in the forward turbine mode, which is used 45 % of the operational time [5]. In the backward turbine mode, the peak efficiency is 73 %. Efficiencies are even lower in the forward and backward pumping modes, at 66 % and 58 %, respectively [9].
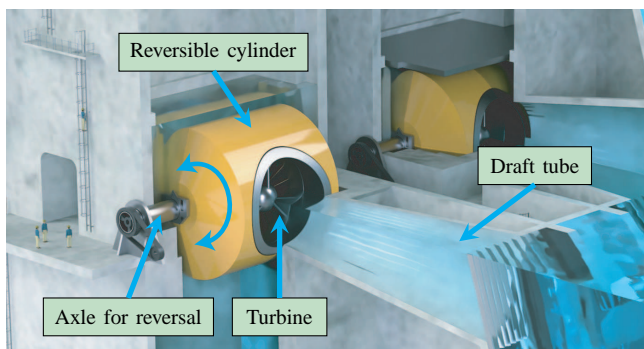


Fig. 2. Concept of the turbine that is installed in a reversible cylinder (Figure courtesy of Tidetec AS)

In the Safe*Coast project, a turbine is being developed that seeks to mitigate the problem of suboptimal efficiency in two of the four possible operation modes. The idea is to install the turbine in a reversible cylinder. To change the flow direction, the cylinder is turned 180°, reversing the whole turbine altogether, as depicted in Figure 2. Thus, equal efficiencies will be reached for both flow directions, as the turbine is always operating in the preferred direction for which it can be optimized. To find a suitable turbine configuration, a set of characteristics was evaluated in a parameter study. The results of this study were presented in an earlier article [10]. Subsequently, it was decided to design a speed variable turbine with adjustable guide vanes and fixed runner blades. To obtain a compact turbine design that can be fitted into the reversible cylinder, a ring generator similar to the Straflo-design used in the Annapolis Tidal Power Plant is used.

This paper describes the design and optimization process of the new turbine and the obtained turbine characteristics. It proposes a compact turbine design that fits into a reversible cylinder, is highly efficient, and has excellent operating properties.

## II. METHODOLOGY

The methodology for generating the geometry of the turbine and performing the simulations is described in the following section. The numerical simulations were carried out using ANSYS CFX 17.2, which is capable of parallelization and parameterization. The simulation of rotating machines such as pumps and turbines can be performed using a turbo mode. This facilitates pre-processing, for instance the mesh generation and setup of interfaces, as well as post-processing for example by drawing blade loading or blade-to-blade plots.

### A. Unit speed and unit discharge

For the representation of the turbine performance characteristics at different operating points the unit quantities $Q_1'$ and $n_1'$ are used. These values represent the characteristics of a geometrically similar turbine with a runner diameter of

$D_E = 1\,\mathrm{m}$, operating at a head of $H_E = 1\,\mathrm{m}$. This allows for a comparison of different turbine types and sizes and different operating points [11]. The unit discharge $Q_1'$ and the unit speed $n_1'$ are defined as follows,

$$Q_1' = \frac{Q}{D^2 \cdot \sqrt{H}} \cdot D_E{}^2 \cdot \sqrt{H_E} \quad [\mathrm{m^3/s}] \tag{1}$$

$$n_1' = \frac{n \cdot D}{\sqrt{H}} \cdot \frac{\sqrt{H_E}}{D_E} \qquad [\mathrm{min^{-1}}] \tag{2}$$

where $Q$ $[\mathrm{m^3/s}]$ is the discharge through the turbine, $D$ [m] is the runner diameter of the turbine, $H$ [m] is the hydraulic head, $n$ $[\mathrm{min^{-1}}]$ is the rotational speed of the runner, $D_E$ [m] is the unit diameter of 1, and $H_E$ [m] is the unit head of 1.

### B. Turbine geometry

For the design of the turbine geometry, the CAD software CATIA was used. The meridional section, i.e. the hub and shroud contours, the draft tube, as well as runner and guide vane profiles and the mechanical design were created from scratch. Instead of a classical bulb turbine design, a Straflo approach was chosen in order to reduce the axial length of the turbine as much as possible. By placing the generator on the periphery of the runner, the whole generator bulb that usually makes this kind of turbine quite long can be dispensed with. Normally, the length of a turbine bulb is approximately 2.3 times the runner diameter [4]. In the current design this length was reduced significantly to less than 0.9 times the runner diameter, making the turbine very compact. The overall turbine geometry was split into four numerical domains, namely the inlet domain, the guide vanes domain, the runner domain and the outlet domain(see Figure 3).

*1) Turbine inlet and draft tube:* One constraint during the design of the turbine was that the turbine inlet and the draft tube have to be a mirror image of each other. When the flow direction between the sea and the basin is reversed, the cylinder rotates 180° and therefore the inlet and outlet geometries exchange functions. In low head applications, the functionality of the draft tube is very important for the turbine to work efficiently [12]. It was therefore decided to design the draft tube as a conventional conical diffuser with a moderate area ratio, thus having a low risk of boundary layer separation
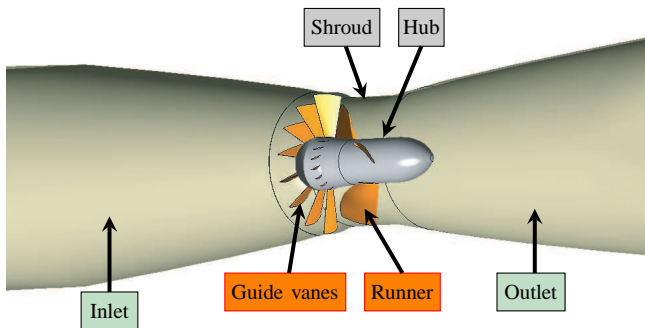


Fig. 3. Cross section through the turbine geometry shown in CFD-Post

as described in literature [12]. The draft tube geometry was then mirrored and also used as inlet geometry. The transition from the circular cross section to a rectangular one starts approximately halfway along the draft tube.

*2) Guide vanes:* The stator of the turbine consists of 16 adjustable guide vanes. During optimization, vanes with curvatures from 20° to 45° were investigated. The thickness distribution and overall thickness of the blades were examined as well. The guide vane profiles were created using ANSYS BladeGen. In the closed position, the guide vanes shut completely, and therefore are able to stop the flow entirely.

*3) Runner:* The turbine runner consists of three fixed blades and has a hub ratio of 0.35. A ring connects the blades on the periphery and acts as a mount for the generator rotor. This ring and the gap between the generator rotor and stator were not taken into account in the numerical simulations. The runner geometry was created in ANSYS BladeGen by defining profiles on seven layers between the hub and shroud. On each layer, the angle and thickness distribution was defined separately. The leading and trailing edges shape was varied also from hub to shroud.

### C. Parameterization

ANSYS CFX allows for a parameterization of the whole simulation setup. Selected input values such as guide vane angle, rotational speed, mass flow rate and pressure at boundary conditions were parameterized in order to automate simulation runs. Those values fed into a list of simulations – the so called design points. For each design point, the input parameters are taken from the list and applied in the pre-processing. Next, the flow simulation is computed until the equation residuals fall below a specified value, or a predefined number of time steps is reached. Upon completion, the post-processing module is executed and output parameters are calculated. Those parameters are, for example, the total and static head, mechanical and fluid power, as well as efficiency. Those values are then stored in the list of design points and can be used to interpret and evaluate the solution.

As an example of an output parameter, the calculation of the turbine efficiency is shown here. It is obtained by dividing the mechanical power at the runner blades by the power of the fluid,

$$\eta = \frac{T \cdot \omega}{\rho \cdot Q \cdot g \cdot H} = \frac{T \cdot \omega}{Q \cdot (p_{t,in} - p_{t,out})} \quad [-] \tag{3}$$

where $T$ [Nm] is the torque around the main turbine axis, $\omega$ [rad/s] is the angular velocity, $\rho$ $[\mathrm{kg/m^3}]$ is the density of the fluid, $Q$ $[\mathrm{m^3/s}]$ is the volume flow rate, $g$ $[\mathrm{m/s^2}]$ is the gravitational acceleration, $H$ [m] is the hydraulic head and $p_{t,in}$ [Pa] and $p_{t,out}$ [Pa] are the total pressures at the inlet and outlet. The total pressure was determined by mass flow averaging on two planes in the cross section of the turbine at a distance of $\pm 0.25\,\mathrm{m}$ upstream and downstream of the runner center. Deriving the output parameters at a specific guide vane angle and a number of rotational speeds of the runner allowed to numerically derive a braking curve. Its name comes from

physical model tests where the braking momentum of the generator is increased stepwise while maintaining the guide vane angle of the turbine and the head acting on it. As the braking momentum increases, the runner speed decreases. At each step, the power, head, runner speed and momentum are measured, from which the unit quantities can be calculated. By measuring braking curves at different guide vane and runner blade angles (if applicable), a hill chart of the turbine can be derived [13].

### D. Meshing and mesh resolution

The inlet and draft tube domains were meshed using the ANSYS Meshing application. The resulting mesh is unstructured and consists of hexahedral, tetrahedral and pyramidal elements. Prism layers were introduced at all surfaces in order to adequately model the boundary layer. However, the number and growth rates of the prism layers varied between the different locations.

The guide vane and runner domains were meshed using TurboGrid, which is a specialized tool for the meshing of turbomachinery components. It creates a mesh for the passage between the blades, consisting solely of hexahedral elements. The mesh was refined near the leading and trailing edges using the edge block split method.

A detailed view of the runner mesh is given in Figure 4. It shows the quadrilateral faces of the hexahedral elements on the blade and hub surface as well as the y$^+$ distribution on the two surfaces. In order to find a good compromise between simulation time and accuracy, a mesh independence study was conducted. For the optimization process, comparatively coarse meshes were used. Once the simulation results showed good
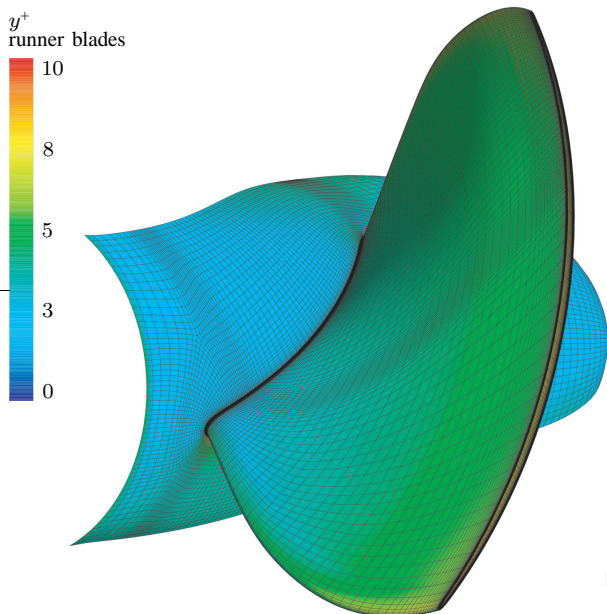
turbine characteristics, high-resolution meshes were used for verification.

Table II shows a summary of the characteristics for the four mesh domains of a high-resolution mesh. Generally, the differences between the coarse and the fine meshes were small.

TABLE II
CHARACTERISTICS OF THE FOUR DOMAIN MESHES (HIGH RESOLUTION)

| Domain | Type | Max. $y^+$ | Exp. rate | Elements |
|---|---|---|---|---|
| Inlet | hex, tet, pyr | 13 | 1.20 | ~530,000 |
| Guide vanes | hex only | 6 | 1.13 | ~650,000 |
| Runner | hex only | 15 | 1.16 | ~1,100,000 |
| Outlet | hex, tet, pyr | 5 | 1.20 | ~450,000 |

### E. Turbulence modeling and $y^+$

For adequate modeling of the boundary layer, it is important that the mesh near the walls is properly sized. A good measure for this is the dimensionless wall distance $y^+$. It can be calculated by

$$y^+ = \frac{u_* \cdot y}{\nu} \quad [-] \tag{4}$$

where $u_*$ [m/s] is the friction velocity at the nearest wall, $y$ [m] is the distance to the nearest wall and $\nu$ [m$^2$/s] is the local kinematic viscosity [14]. Generally, the $y^+$-values were kept below 100 while on the runner and guide vane planes the $y^+$-values were in the range of 5 to 10.

Menters Shear Stress Transport (SST) model, a two equation eddy-viscosity model, was used as turbulence model. It combines the advantages of both the $k$-$\omega$ and the $k$-$\epsilon$ models by using the first to model the flow near the wall and the latter in the free stream [15].

ANSYS CFX uses two methods to compute the flow in the boundary layer, depending on the $y^+$-value. For $y^+$ below 2, a strict low Reynolds implementation is applied, where the details of the boundary layer are resolved. With $y^+$-values larger than 30, logarithmic wall functions are used. For $y^+$ values between 2 and 30 the two approaches are blended in order to allow for a smooth transition [16].

### F. Boundary conditions

In order to solve the equations of fluid flow, boundary conditions have to be set at the boundaries of the different domains. Three types of boundary conditions are relevant in this study: fluid boundaries, where the flow enters and exits the computation domain; solid boundaries, where the flow contacts solid bodies and fluid-fluid-interfaces where the flow passes from one domain to another.

*1) Inlet boundary condition:* A mass flow rate boundary condition was used at the inlet, where water enters the computational domain. A positive value for the mass flow rate defines a mass flux entering the domain, whereas a negative value defines a mass flux leaving the domain. The total pressure with



Fig. 4. Mesh of the runner with $y^+$-values on the blade and hub surfaces

this kind of boundary condition may vary. The inlet direction was set at right angles to the boundary and the inlet turbulence intensity was set to medium (5 %).

*2) Outlet boundary condition:* At the opposite side, where the flow predominantly leaves the domain, an opening boundary condition was defined. For the opening, a relative static pressure was defined, which is used when the flow is leaving the domain. However, the boundary condition also allows for a flow of water into the domain, in case of recirculation. In this case, the defined pressure is taken as a total pressure. The inlet direction of the flow was set to normal to the boundary.

*3) Stationary Walls:* On all the domains that represent the stationary turbine geometry, such as the hub and shroud or the draft tube, wall boundary conditions were set. Those boundaries are solid and therefore impermeable for the flow. The type of the walls was set to no slip, which means that the flow velocity at the wall is zero. The velocity profile immediately next to the wall and towards the free stream is dependent on the wall roughness, which was set to smooth in our case.

*4) Rotating wall:* The purpose of the runner domain was to simulate the revolving rotor. Therefore the frame of reference was rotating in all simulations. However, in reality, the walls next to the runner are stationary. In order to represent the shroud correctly, the option "counter rotating wall" was used for the wall velocity at the corresponding boundary. The counter rotating wall velocity in respect of the rotating frame of reference simulates a stationary wall. In fact, this neglects the ring of the rim generator around the runner. However, the length of this ring is short in comparison to the whole length of the runner domain and the inaccuracy is smaller, as if the whole shroud was rotating. The hub is quite long and therefore was simulated as stationary with respect to the runner domain, or rotating in respect to the stationary frame of reference.

### G. Analysis types

Steady state simulations were carried out during the first steps of the optimization process. This saved a lot of computational effort and made it possible to study an extensive set of geometries. Once the final geometry was found, transient simulations were carried out to verify the results and to examine transient effects.

*1) Steady state simulations:* In the steady state simulations, both the flow in the guide vane and in the rotor domain were simulated within one blade channel instead of the whole circumference of the turbine. Thus, only a sector of the full circle of each domain was simulated. The number of mesh elements was reduced by 93.75 % in the guide vane domain and 66 % in the runner domain. Rotational periodic interfaces were used to represent the adjacent blade channels. To establish the frame and pitch change between the stationary and rotating domains, stage interfaces were used.

*2) Transient simulations:* In the transient simulations, the flow in the complete domain, i.e. all sixteen guide vane passages and all three runner passages was simulated. Transient rotor-stator interfaces connected the four domains. The runner

mesh was rotated between the time steps according to the respective rotation speed and time step size. The number of elements of the whole setup and consequently the computation time was considerably higher than in the steady state simulations. A simulation of the whole turbine representing two seconds of operation took roughly eight days to compute with 16 physical cores clocked at 3.5 GHz. This type of simulation calculates the actual flow very precisely. In particular, the draft tube flow and flow separations are resolved better than in the steady state simulations.

### H. Convergence

All simulations were run until convergence was reached. This was checked by monitoring the equation residuals as well as selected monitor values like head and efficiency. In some simulations, the monitor values started to fluctuate periodically after a number of time steps. Flow separation in small areas at the guide vanes or the draft tube was identified as the main cause. Once these fluctuations reached a constant frequency and magnitude, the simulations were stopped, as transient effects like periodic vortex shedding cannot be resolved in steady state simulations. However, the simulation results are still considered valid as the fluctuation magnitude was generally very low. In the transient simulations, all physically relevant effects were resolved and convergence was reached in all cases.

### I. Optimization

In the following, a brief description of the optimization process and the design goals will be given. As already mentioned, much of the setup was automated by defining design points in order to conduct a great number of simulations. However, after each modification of the geometry, the results were analyzed and changes were made accordingly in an effort to improve the performance. Overall, more than 80 geometry combinations were investigated. The result parameters taken into account were the unit discharge, unit speed, efficiency, exit swirl distribution, and cavitation properties. Unit discharge and unit speed were calculated according to Equations 1 and 2 after the head was determined on the measurement planes. Efficiency was calculated according to Equation 3. The power, head and efficiency of a turbine can be determined based on Euler's turbine equation [13]

$$Y_{th} = H_{th} \cdot g = c_{2u} \cdot u_2 - c_{1u} \cdot u_1 = \Delta(u \cdot c_u) \ [\text{J/kg}] \ (5)$$

where $Y_{th}$ [J/kg] is the specific work, $H_{th}$ [m] is the theoretical pressure head, $g$ [m$^2$/s] is the gravitational acceleration, $c_{1u}$ and $c_{2u}$ [m/s] are the circumferential components of the absolute velocities at the inlet and outlet, respectively and $u_1$ and $u_2$ [m/s] are the blade velocities at the inlet and outlet respectively. The blade velocity $u$ can be obtained by multiplying the radius $r$ with the angular velocity $\omega$ — $u$ and $r$ are therefore directly proportional. Thus, $\Delta(u \cdot c_u)$ can also be expressed as $\Delta(r \cdot c_u)$, which is done in the following.

*1) Inlet swirl:* The inlet and exit swirl distributions were determined on two cross-sectional planes in the turbine at a short distance up- and downstream of the runner. On those planes, lines with constant span were defined. For each location on those lines the magnitude of $r \cdot c_u$ was calculated using the local radius r and the local circumferential component of the absolute velocity $c_u$. Subsequently, all the local values of $r \cdot c_u$ were averaged on each line of constant span.

The inlet swirl is generated by the guide vanes and can be varied by changing their incidence and deflection flow angles. The outlet swirl, however, is determined by the runner blades.

In general, it was tried to generate a distribution of $r \cdot c_u$ at the inlet, which has a linear trend from the hub (span = 0) to the shroud (span = 1). A distribution with a small gradient was aimed for, which is challenging in the case of axial turbines. In traditional Kaplan or bulb turbines, the cylindrical or strongly conical shape of the guide vane apparatus permits making use of the law of conservation of angular momentum to obtain a nearly uniform distribution of $r \cdot c_u$. However, in the present case, due to the required symmetry of in- and outlet, it was not possible to give the guide vane apparatus a pronounced conical shape.

*2) Outlet swirl:* Concerning the outlet swirl, a distribution with some residual swirl near the outer wall and very low or slightly negative swirl near the center line was aimed for. High outlet swirl means an energy loss, but a certain amount of exit swirl was identified as stabilizing the flow in the diffusor. As in the inlet, a linear distribution is desirable.

The inclination of the outlet swirl distribution should follow that of the inlet distribution to ensure that a similar amount of Euler head $\Delta r \cdot c_u$ is extracted over all spans. Neglecting this condition may lead to compensation currents, which negatively affect the distribution of the meridional velocity at the runner outlet, leading to an increase of the draft tube losses and a reduced turbine efficiency.

*3) Meridional velocity distribution:* The meridional velocity $c_m$ is the component of the velocity perpendicular to the cross section of the turbine. It is therefore a measure for the local mass transport through the turbine. It should in general be equal in magnitude from hub to shroud, so that the flow through the turbine is well balanced, i.e. the meridional velocity distribution should be constant.

*4) Cavitation:* Figure 5 shows the blade loading of a runner developed early in the optimization process.

The depicted lines represent the static pressure $p$ on the pressure and suction side of one runner blade at cylinder sections on different spans. At a span of 0.95, i.e. at the tip of the rotor, there is a very sharp negative pressure spike at the leading edge. Negative pressures to this extent indicate that leading edge cavitation and subsequent cavitation erosion might occur.

One of the design targets was to find a blade shape that is free from cavitation in a wide range of operating points. The geometry was therefore changed until a satisfactory geometry of the runner blades was found.
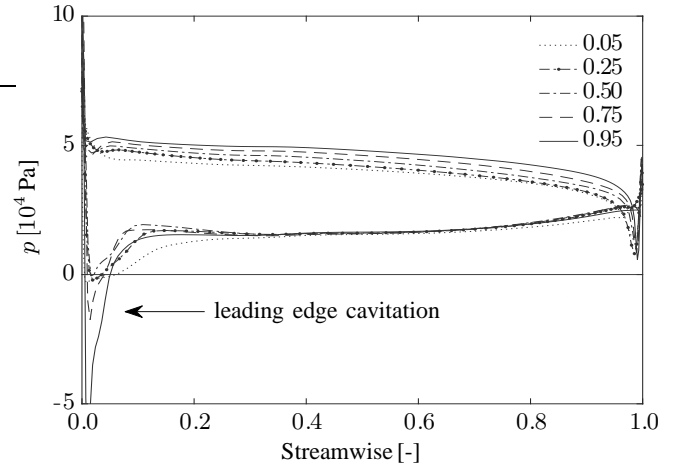


Fig. 5. Pressure on blades of a premature runner at different spans
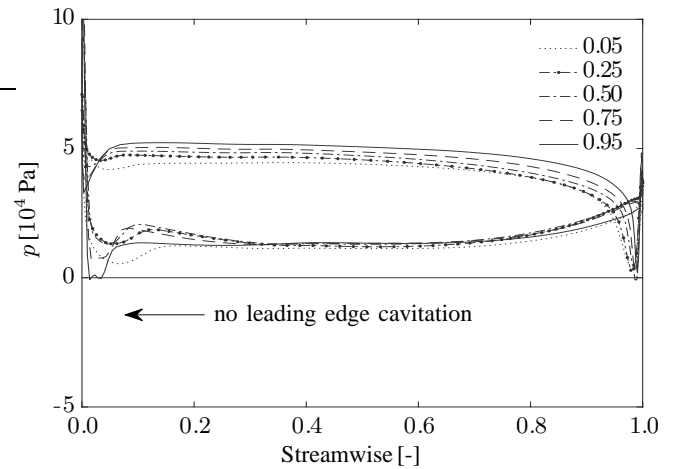


Fig. 6. Pressure on blades of the final runner at different spans

Figure 6 shows the blade loading chart of the final runner geometry in the rated operating point. It was possible to eliminate the zone of very low pressures and it is therefore expected that the runner will operate without cavitation.

## III. RESULTS

In the following section, the results of the simulations are described and evaluated.

*A. Turbine mode*

Firstly, the characteristics in the turbine mode are shown.

*1) Efficiencies:* The resulting efficiencies at different guide vane angles $\gamma$ and different values of the unit speed $n_1'$ are depicted in Figure 7.

Overall, the resulting efficiencies are greater than 85 % for unit speeds of $n_1' = 100 - 250 \, \text{min}^{-1}$. The best efficiency in the turbine mode is $\eta = 92.5 \%$ at a guide vane angle of $\gamma = 0°$ and a unit speed of $n_1' = 150 \, \text{min}^{-1}$. The efficiencies for guide vane angles of $\gamma = +0°$, $+2.5°$ and $+5°$ are very similar over a wide range of unit speeds, while they decrease for values outside of this range.

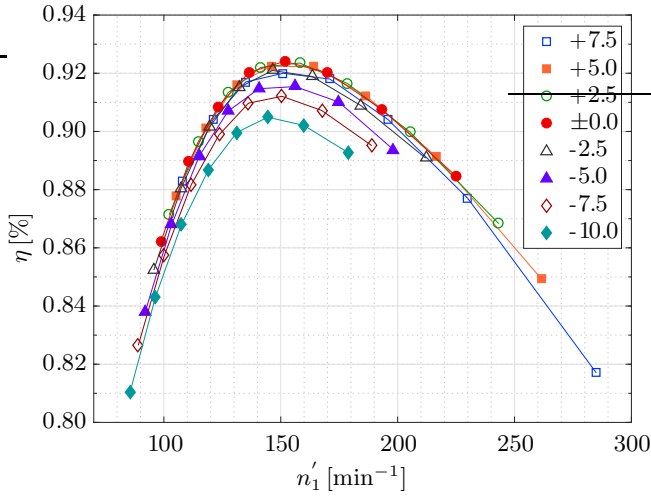Fig. 7. Efficiency at guide vane angles $\gamma$ from +7.5° to -10°



Fig. 9. Distribution of meridional velocity $c_m$ upstream and downstream of the runner in turbine mode

*2) Unit discharge:* Adjusting the guide vane angle also affects the unit discharge $Q'_1$. Figure 8 shows the unit discharges at different guide vane angles and unit speeds. Generally, the unit discharge increases with greater unit speed. Moreover, as expected, it is also higher for greater guide vane opening angles. Overall, the unit discharges are in a range of $Q'_1 = 1.8 - 3.3\,\mathrm{m}^3/\mathrm{s}$ for unit speeds of $n'_1 = 100 - 250\,\mathrm{min}^{-1}$. The unit discharge $Q'_1$ at the best efficiency point is $2.3\,\mathrm{m}^3/\mathrm{s}$, however, higher unit discharges can be reached at reasonable efficiencies.
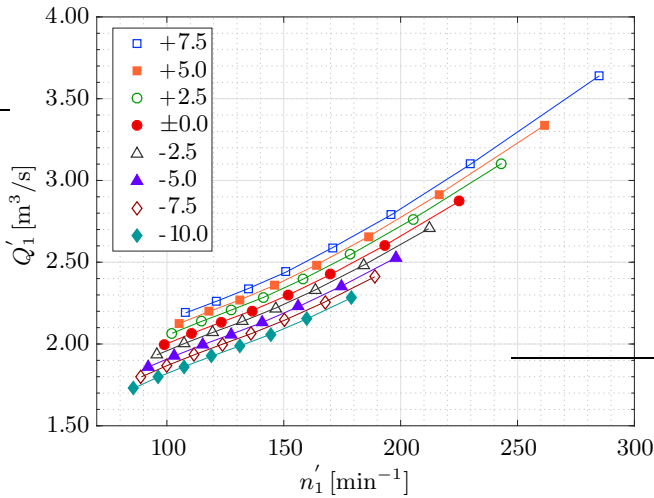


Fig. 8. Unit discharge at guide vane angles $\gamma$ from +7.5° to -10°

*3) Meridional velocity distribution:* The distribution of the meridional velocity $c_m$ in turbine mode is depicted in Figure 9. Upstream of the runner, i.e. between the guide vanes and the runner, the meridional velocity has a very balanced distribution with a magnitude of $c_m \approx 6\,\mathrm{m}/\mathrm{s}$ between the hub and the shroud. Near the inner and outer wall surface, the flow velocity drops to zero, as expected. The velocity distribution alters when passing the runner, but still has a relatively even distribu-
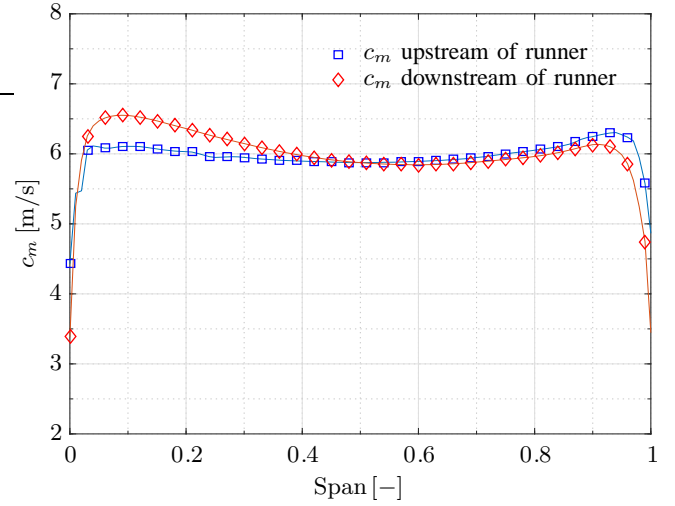
tion downstream of the runner. The flow is diverted somewhat towards the hub with a maximum of $c_m = 6.5\,\mathrm{m}/\mathrm{s}$ at a span of 0.1. Generally, the flow velocities are slightly higher at this location. This is attributed to continuity, as the cross section of the turbine decreases slightly from upstream to downstream.

*4) Swirl distribution:* The outlet swirl distribution is strongly dependent on the runner speed and therefore on the operating point. The distribution of $r \cdot c_u$ is depicted in Figure 10 for the rated operating point. Upstream of the runner, the distribution has a linear gradient from hub to shroud. As the flow progresses through the runner, it performs mechanical work on the runner blades and the hydraulic head is reduced. This reduction is reflected in the drop of $r \cdot c_u$ from upstream to downstream of the runner. As anticipated, the swirl near the hub is slightly negative and zero at a span of 0.2. Directly at the hub, the swirl increases, which is induced by the rotating
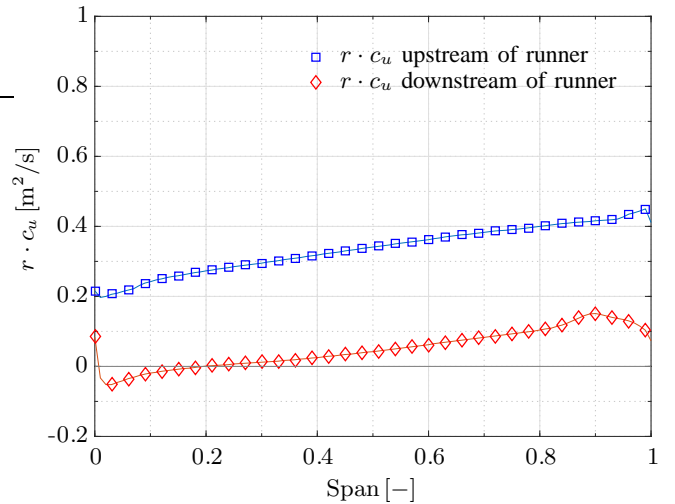


Fig. 10. Distribution of $r \cdot c_u$ upstream and downstream of the runner in turbine mode
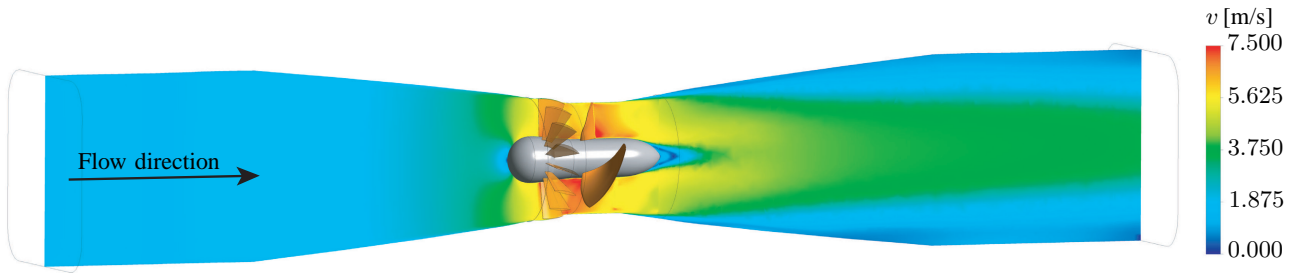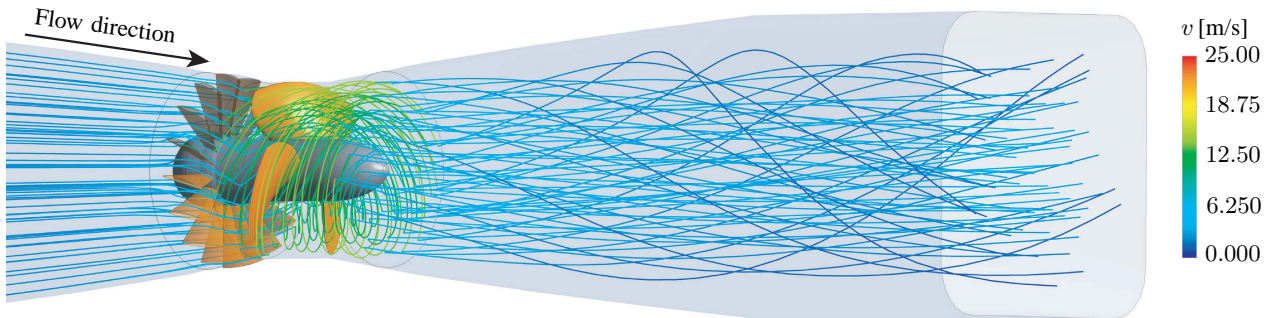
Fig. 11. Velocity distribution in turbine mode



Fig. 12. Streamlines in inlet, guide vanes, runner and draft tube in turbine mode

surface of the hub. Towards the shroud, the swirl also increases with an almost linear gradient.

The general flow through the turbine in turbine mode is depicted in Figures 11 and 12.

*5) Cavitation properties:* The final runner is expected to have good cavitation properties in the turbine mode. The blade loading chart depicted in Figure 6 shows the pressure distribution on the blade surface at different spans.

In streamwise direction, the pressures on each span are quite constant. At the leading edge, there are moderate pressure spikes with a short streamwise extension. Those come from a small incidence angle at the normal operating point, and will not lead to cavitation when operating the turbine in conventional pressure levels.

With slower rotation speeds of the runner, this incidence angle increases, which also leads to lower pressures at the leading edge. The crossing of the pressure lines at the trailing edge is assumed to come from a deviation angle as described in [17].

### B. Pumping mode

Unlike in the turbine mode, there is only one operating point in the pumping mode that results in favorable kinematic conditions. This is due to the fact that the runner is now situated upstream of the guide vanes and no inlet swirl is present. In order to avoid too high an angle of attack, the runner speed has to be chosen accordingly. While passing the runner, the pressure of the flow is increased, as is the

swirl. Next, the flow passes the guide vanes downstream of the runner. By choosing an appropriate guide vane angle, the swirl is reduced again and its kinetic energy is converted into static pressure.

*1) Efficiency:* In general, the efficiency in the pumping mode was found to be lower than in the turbine mode. The peak efficiency derived by Equation 3 is 87 % at a unit speed of $n'_1 = 230\,\mathrm{min}^{-1}$. However, when the energy losses in the turbine inlet and the draft tube are taken into account, the total efficiency is 77 %. This is mainly caused by a suboptimal function of the draft tube in the pumping mode. As the flow leaves the guide vanes, it has a low velocity in the center of the turbine. Therefore only a part of the kinetic energy is regained as pressure in the draft tube. However, as the pumping operation time in a barrage scheme is comparatively short and the process takes place under low heads, the pumping efficiency is less critical than the turbine efficiency. The flow field in the pumping mode is depicted in Figure 13.

*2) Unit discharge:* The unit discharge in pumping operation is $Q'_1 = 3.15\,\mathrm{m^3/s}$ at a unit speed of $n'_1 = 230\,\mathrm{min}^{-1}$. It is higher than in the turbine mode, which is a favorable property that was sought for in the optimization. For tidal power plants, a high unit discharge in pumping mode is desirable, as the pumping heads are usually quite small and as much water as possible should be moved.

*3) Meridional velocity distribution:* The distribution of the meridional velocity $c_m$ in pumping mode is depicted in Figure 14. The meridional velocity has an almost constant
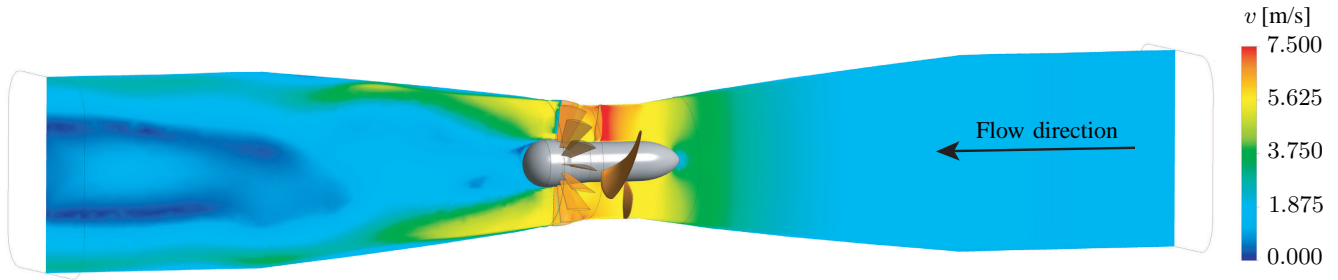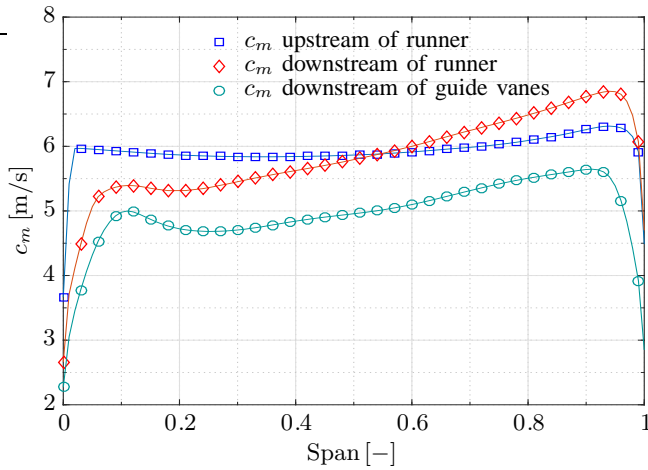
Fig. 13.   Velocity distribution in pumping mode

magnitude of $c_m \approx 6\,\mathrm{m/s}$ upstream of the runner, just as in the turbine mode. Again, the meridional velocity drops towards zero at the hub and shroud surfaces.
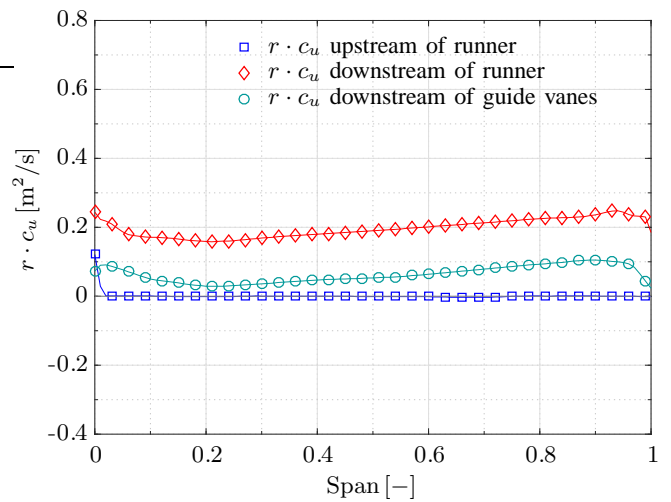
Downstream of the runner, or upstream of the guide vanes, the flow is slightly unbalanced with $c_m = 5.25\,\mathrm{m/s}$ near the hub (span = 0.2) and $c_m = 6.8\,\mathrm{m/s}$ near the shroud (span = 0.9). The difference in magnitude is $\Delta c_m = 1.55\,\mathrm{m/s}$.

While passing the guide vanes, the distribution is re-balanced to some degree, which is reflected in the velocity distribution downstream of the guide vanes. In this location the transport velocities range from 4.6 m/s near the hub to 5.6 m/s near the shroud, thus $\Delta c_m = 1\,\mathrm{m/s}$. The overall meridional velocities downstream of the guide vanes are reduced, as the cross section of the turbine is larger at this position. Ideally, the meridional velocity should be balanced even further, with higher velocities near the hub, in order to ensure proper conditions for the draft tube flow. The general flow through the turbine in pumping mode is depicted in Figure 13.



Fig. 14.   Distribution of meridional velocity $c_m$ upstream and downstream of the runner and downstream of the guide vanes in pumping mode

*4) Swirl distribution:* The distribution of $r \cdot c_u$ in pumping mode is depicted in Figure 15. The inlet swirl upstream of the runner is zero over the whole range between hub and shroud, as expected. Only directly at the hub is the water drawn into

rotation by the moving hub surface. Downstream of the runner, the flow has a high level of $r \cdot c_u$ on all spans with a relatively balanced distribution of approximately $0.2\,\mathrm{m^2/s}$.



Fig. 15.   Distribution of $r \cdot c_u$ upstream and downstream of the runner and downstream of the guide vanes in pumping mode

The swirl distribution is slightly skewed with a higher magnitude near the shroud. After passing the guide vanes, most of the swirl is removed again as the flow is straightened. Its distribution downstream of the guide vanes is similar in shape but the overall magnitudes are smaller. Some residual swirl remains throughout all spans.

*5) Cavitation properties:* The final runner is also expected to have good cavitation properties in the pumping mode. The blade loading chart depicted in Figure 16 shows the pressure distribution on the blade surface at different spans.

In streamwise direction, the pressures are quite constant for spans greater than 0.5. At lower spans, the pressure difference decreases in streamwise direction from halfway along the blade. At the leading edge, there are moderate negative pressure spikes with a very short streamwise extension. Those again are caused by a small incidence angle, and will not lead to cavitation. A deflection angle at the trailing edge causes a crossing of the pressure lines.
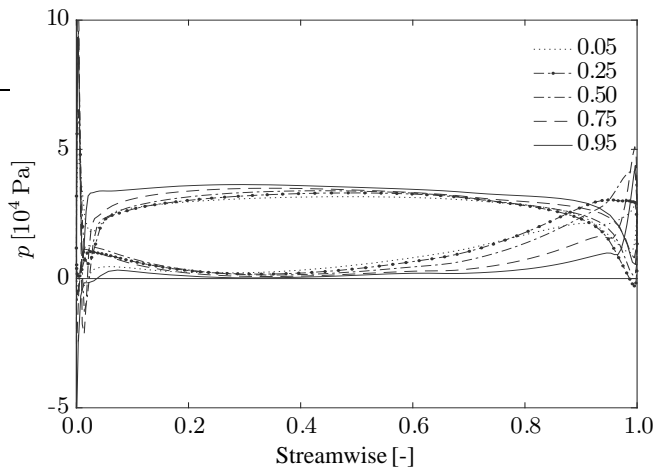
Fig. 16.  Pressure on blades in pumping operation at different spans

## IV. Conclusion

The simulations show that the turbine performs well in both operating modes. The maximum efficiency in turbine mode is very high, as is the unit discharge. Moreover, the turbine has safe cavitation properties. In the pumping mode, the efficiency is satisfactory as well. The high unit discharge achieved is very favorable for operating schemes that make use of pumping.

The authors conclude that the presented design may contribute to an increase in tidal power production should the concept prove to be economically feasible.

Thanks to the positive simulation results it was decided to take the next step and conduct model tests in a closed loop test rig at our lab. The measurements will be used to verify the simulations and to give insight into future optimization potential. They will also provide data on the friction losses in the generator gap. A model turbine was manufactured and will soon be tested.

Details on the test rig, the implementation of the model turbine and the planned measurement program are available in article published in the conference proceedings at hand [18].

## Acknowledgment

## References

[1]  R. H. Charlier, *Ocean energy*.  Berlin: Springer, 2009.
[2]  R. Spain, "A Possible Roman Tide Mill." [Online]. Available: http://www.kentarchaeology.ac/authors/005.pdf
[3]  A. C. Baker, *Tidal power*, ser. IEE energy series.  London, U.K.: P. Peregrinus, 1991, vol. 5.
[4]  R. H. Clark, *Elements of tidal-electric engineering*.  Hoboken, NJ, USA: Wiley-IEEE, 2007.
[5]  L. B. Bernshteĭn, *Tidal Power Plants*.  Seoul, Korea: Korea Ocean Research and Development Institute, 1996.
[6]  "Kislogubskaya tidal," 2011. [Online]. Available: http://blog.rushydro.ru/?p=4250(inrussian)
[7]  Y. H. Bae, K. O. Kim, and B. H. Choi, "Lake Sihwa tidal power plant project," *Ocean Engineering*, vol. 37, no. 5-6, pp. 454–463, 2010.
[8]  W. Zhengwei, Y. Xiaosheng, and X. Yexiang, "Hydraulic performance optimization of bidirectional tidal power turbine," *China Journal of Drainage and Irrigation Machinery Engineering*, vol. 5, pp. 417–421, 2010. [Online]. Available: http://en.cnki.com.cn/Article_en/CJFDTOTAL-PGJX201005012.htm
[9]  D. Aelbrecht and L. Derlot, "La Rance Tidal Power Plant: past, present and future," Brest, 15 Octobre 2014. [Online]. Available: http://www.seatechweek.com/images/demo/slider4/MEB_pjt_1_EDF_LaRance_maremoteu
[10]  S. Hötzl, T. Schechtl, and W. Knapp, "Development of a turnable turbine for use in barrage type tidal power plants," in *Wasserbau - mehr als Bauen im Wasser*, ser. Berichte des Lehrstuhls und der Versuchsanstalt für Wasserbau und Wasserwirtschaft, P. Rutschmann, Ed.  München: TUM, 2016. [Online]. Available:  http://www.freunde.wb.bgu.tum.de/fileadmin/w00bol/www/Symposium_2016/Beitraege_Wallgau2016/78_-_Hoetzl.pdf
[11]  J. Giesecke and E. Mosonyi, *Wasserkraftanlagen: Planung, Bau und Betrieb*.  Berlin, Heidelberg: Springer-Verlag Berlin Heidelberg, 2009.
[12]  S. Deniz, M. Bosshard, J. Speerli, and P. Volkart, *Saugrohre bei Flusskraftwerken*, ser. VAW Mitteilungen.  Zürich: Versuchsanstalt für Wasserbau Hydrologie und Glaziologie der ETH Zürich, 1990, vol. 106.
[13]  H. Sigloch, *Strömungsmaschinen: Grundlagen und Anwendungen ; mit 36 Tabellen*, 4th ed.  München: Hanser, 2009.
[14]  H. Schlichting and K. Gersten, *Grenzschicht-Theorie*, 10th ed.  Berlin: Springer, 2006.
[15]  F. R. Menter, "Two-equation eddy-viscosity turbulence models for engineering applications," *AIAA Journal*, vol. 32, no. 8, pp. 1598–1605, 1994.
[16]  "ANSYS® CFX, Release 17.2, Help System, Modeling Guide."
[17]  M. Hutter, "Numerische Untersuchung und Optimierung der Leitrad-Laufrad-Saugrohrinteraktion bei Axialturbinen," Dissertation, Technische Universität München, München, 15. September 2015.
[18]  T. Schechtl, S. Hötzl, P. Rutschmann, and W. Knapp, "Development of a Low Head Tidal Turbine Part 2: Test Rig and Model Turbine Design," in *Proceedings of the European Wave and Tidal Energy Conference 2017*, Cork, Ireland, 2017.